Journal of Catalysis **190,** 128–143 (2000)
doi:10.1006/jcat.1999.2743, available online at http://www.idealibrary.com on IDEAL®

Structure, Energetics, and Electronic Properties of the Surface of a Promoted MoS_2 Catalyst: An ab Initio Local Density Functional Study

P. Raybaud,* J. Hafner,‡ G. Kresse,‡ S. Kasztelan,† and H. Toulhoat*

*Division Informatique Scientifique et Mathématiques Appliquées, Institut Français du Pétrole, 92852 Rueil-Malmaison Cedex, France; †Division Cinétique et Catalyse, Institut Français du Pétrole, 92852 Rueil-Malmaison Cedex, France; and ‡Institut für Materialphysik and Center for Computational Materials Science, Universität Wien, Sensengasse 9, A-1090 Wien, Austria

Received July 6, 1999; revised October 26, 1999; accepted October 27, 1999

The determination of the local structure of cobalt- or nickel-promoted MoS_2-based hydrodesulfurization catalysts is of interest for understanding the mechanism leading to an increased activity brought by cobalt or nickel, the so-called synergetic effect. For that reason, we carried out ab initio calculations using density functional theory under the generalized gradient approximation for periodic systems. The edge substitution model emerges as the most stable structure and provides an excellent agreement with local structures experimentally determined on real catalysts by *in situ* extended X-ray absorption fine structure. We studied the adsorption of sulfur on the active edge surface of the promoted MoS_2 catalyst and determined the equilibrium coverage under sulfiding conditions. It is demonstrated that the incorporation of promoter atoms has a strong influence on the sulfur–metal bond energy at the surface and in particular leads to a reduction of the equilibrium S coverage of the active metal sites. A comparative study on the effects of Co, Ni, and Cu atoms as promoters was performed. Detailed results on the surface electronic structure of promoted MoS_2 are presented.

Key Words: **hydrodesulfurization catalysts; molybdenum disulfides; CoMoS; NiMoS; promoter location; surface structure; density functional calculations.**

I. INTRODUCTION

For many years CoMo(W)S and NiMo(W)S catalysts have been known to be very active in hydrodesulfurization (HDS) reactions. It is well known (1) that the activity of MoS_2 doped with either Co or Ni atoms is substantially higher than the activity of either Mo, Co, or Ni sulfides alone. Nevertheless, many issues concerning the microscopic mechanism of the catalytic process, and in particular the role of Co or Ni in enhancing the reactivity of pure MoS_2 or WS_2 catalysts, are poorly understood.

An understanding of the synergetic effect requires the answers to two questions. The first one, related to the surface structure, is about the exact location and the local environment of the promoter atoms. Once the location of the promoter is known, its effect on the reactivity has to be investigated. Many experimental studies have been devoted to this topic, but they were hindered by the difficulty of controlling the simultaneous change of several parameters (sulfur content, particle size of the active phase, promoter content...) depending on the preparation mode or on the conditions of the reaction. Mössbauer studies (2) on cobalt-promoted MoS_2 have shown that cobalt is present in the form of a stable but inactive Co_9S_8 phase, as atoms inserted in the alumina carrier, and in a "CoMoS" phase (3) which was shown to be the active phase. Studies of the reactivity of cobalt-promoted MoS_2 single crystals (4) show that Co tends to be located near the edge planes. Ion scattering spectroscopy (ISS), X-ray photoelectron spectroscopy (XPS), and laser Raman spectroscopy (LRS) (5–7) investigations on unsupported and alumina-supported NiMoS catalysts demonstrated that the nickel content that is favorable for the existence of the NiMoS phase corresponds to an atomic ratio Ni/(Ni + Mo) lower than 0.3. For larger atomic ratios, the inactive Ni_3S_2 phase begins to form and the HDS reactivity decreases. In unsupported systems, this phase may act as a carrier, enhancing the dispersion of the NiMoS phase to some extent (6).

If the existence of an active CoMoS/NiMoS phase is now well established, the precise location of the promoter is still unclear. Several models have been proposed for many years. The oldest one, proposed by Voorhoeve and Stuiver (8, 9) is anterior to the proof of the existence of the CoMoS/NiMoS phase. This model, called the intercalation model, assumes that the promoter is intercalated between two MoS_2 sheets. Farragher and Cossee (10) modified this model, proposing that the promoter should be intercalated in a region close to the surface only. Recent high-resolution electron microscopy (HREM) results of Chianelli *et al.* (11) have been interpreted as indirect evidence for this "pseudointercalation" model.

A second model assumes that the promoter is located in a decorative way on the edges of the MoS_2 sheets, forming adatoms or substituting for Mo atoms. The geometrical model developed by Kasztelan *et al.* (12) has been able to predict consistently the observed activity/composition relationships in these systems. Infrared (IR) studies of NO

0021-9517/00 $35.00

adsorption on supported CoMoS catalysts (13) and EXAFS investigations on carbon- or alumina-supported catalysts (14–18) favor such a model.

For many years theoretical studies have attempted to provide new insights into these systems at a microscopic level. One of the first theoretical investigations was carried out by Harris and Chianelli (19, 20) on transition metal sulfide (TMS) clusters using the SCF-X_α scattered wave method. They studied the periodic trends of TMS catalysts and proposed an interpretation of the synergetic effects in terms of the filling of the TMS d-band. More accurate tools of investigations have been offered by the implementation of the density functional theory (DFT) under the generalized gradient approximation (GGA) coupled with pseudopotential methods on highly powerful computers. Recent work (21–24) on TMS systems has shown that the newest theoretical developments enable us to handle more and more complex systems. Previous theoretical studies (25, 26) have investigated the structural and electronic properties of the $(10\bar{1}0)$ surface (also defined as the "Mo-edge plane") and the (1010) surface (also called the "S-edge plane") exposing coordinatively unsaturated rows of Mo and S atoms in alternating S–Mo–S sandwiches.

The influence of the working conditions on the equilibrium S coverage of the active "edge surfaces" was studied in Ref. (27) through studies on the effect of varying the chemical potential of sulfur in the gas phase. We have shown that the chemical potential of S may influence the local edge structure (sulfur coverage) as well as the shape of the MoS_2 crystallite.

As the debate about the exact location of the promoter is still open, this paper is devoted to the determination of the most stable positions of the promoter in the MoS_2 crystallite by ab initio total energy calculations and local structure optimization. The optimized geometries are compared with the available EXAFS data.

In addition, we investigate in the same spirit as in Ref. (27) to what extent the promoter atoms (cobalt and nickel) modify the sulfur coverage as well as the sulfur–metal bond energies. This is completed by investigations of the surface electronic, structure providing the basis for an interpretation of the promoter effect on the catalytic HDS reaction.

II. METHODS

Our calculations are based on density functional theory, using the local exchange correlation functional proposed by Perdew and Zunger (28), corrected for nonlocal effects by using the generalized gradient corrections developed by Perdew *et al.* (29). The surface is represented by a periodically repeated slab model, using a sufficiently thick vacuum layer to separate neighboring slabs. Electronic eigenstates are expanded in terms of plane waves, using pseudopotentials to describe the electron–ion interactions.

TABLE 1

Parameters Determining the Ultrasoft Pseudopotentials Used: Cutoff Radii $R_{c,l}$ and Augmentation Radii $R_{aug,l}$, $l = s, p, d$

	Co	Ni	Cu
$R_{c,s}$	2.19	2.17	2.21
$R_{c,p}$	2.46	2.43	2.48
$R_{c,d}$	2.46	2.43	2.48
$R_{aug,s}$	2.19	2.17	2.21
$R_{aug,p}$	2.19	2.17	2.21
$R_{aug,d}$	1.99	1.98	2.01

Note. All radii are given in au.

Ultrasoft pseudopotentials (30, 32) are particularly well suited to reduce the cutoff energy for the transition metal pseudopotentials. The solution of the generalized Kohn–Sham equations valid for a system modeled by ultrasoft pseudopotentials is performed using the Vienna ab initio simulation package (VASP) (31, 33, 34). VASP performs an iterative diagonalization of the Kohn–Sham Hamiltonian via unconstrained band-by-band minimization of the norm of the residual vector to each eigenstate and optimized charge density mixing routines. The optimization of the atomic geometry is performed using a conjugate gradient minimization of the total energy, using the exact Hellman–Feynman forces acting on the ions determined in each optimization step. For all transition metal atoms, the atomic reference configuration is $d^{(n-1)}s^1$. For all technical details, including the construction of the ultrasoft pseudopotentials for Mo, S, and H, we refer the reader to our previous publications (25, 26). The parameters determining the ultrasoft pseudopotentials used for Co, Ni, and Cu are reported in Table 1. For a detailed test of the pseudopotentials for Co and Ni, see Moroni *et al.* (35), and for Cu see Kresse and Hafner (32).

Our model for the MoS_2 supercell is similar to the one described in Refs. (25, 27). It is shown in Fig. 1. It consists of two S–Mo–S trilayers, stacked in the *z*-direction. Each sandwich consists of three rows of MoS_6 prisms stacked in the *y*-direction plus rows of terminating Mo atoms on one side of the slab and four rows of prisms in the *x*-direction. This 72-atom unit (composition $Mo_{24}S_{48}$) is periodically repeated in the *x*- and *z*-directions. In the *y*-direction neighboring units are separated by a vacuum layer of 12.8 Å. All calculations have been performed with equilibrium lattice constants of $a = 3.170$ (3.160) Å and $c = 12.584$ (12.294) Å calculated for bulk MoS_2 including generalized gradient corrections (21) (experimental lattice constants in parentheses).

III. RESULTS

A. Localization of the Promoter Atoms

Our aim is to compare by means of total energy calculations the various models for the promoter localization

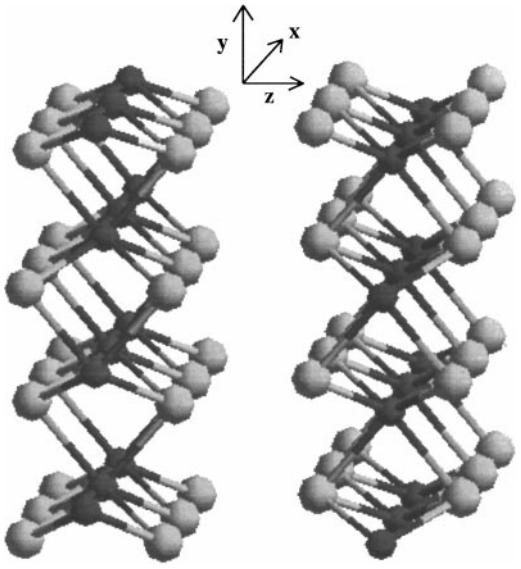

FIG. 1. Perspective view of the supercell used for the MoS_2 edge surface after the 0 K relaxation. This is defined as the stoichiometric as-cleaved surface, with the bare Mo edge and the fully saturated S edge side. Small black balls, Mo atoms; large gray balls, S atoms.

presented in the Introduction. The direct comparison of the total energy after ionic relaxations will allow us to identify the configurations corresponding to the most stable localization of the promoter atom. These comparisons are possible only for systems which have the same composition: the same sulfur content, the same molybdenum loading, and the same promoter loading. Moreover, we compare the fully optimized interatomic distances (Co–S and Co–Mo distances) with EXAFS data.

One of the first ideas is to predict the local environment of the promoter by comparing it with the one of the well-known crystalline phases such as Co_9S_8, CoS (NiAs-type), or CoS_2 (pyrite-type) for cobalt and Ni_3S_2, NiS (NiAs-type), NiS (millerite), and NiS_2 (pyrite-type) for nickel. This approach is often used in X-ray absorption near edge structure (XANES) investigations (36, 37). In two previous papers (21) the structural, electronic, and energetic properties of these crystalline structures were studied in detail. The octahedral environment found in Co_9S_8, CoS (NiAs), and CoS_2 (pyrite) leads to Co–S distances between 2.30 and 2.39 Å, whereas a tetrahedral environment (also present in Co_9S_8) exhibits shorter Co–S distances between 2.13 and 2.21 Å. The nickel monosulfide has also a low-temperature phase, NiS, called the millerite structure with a 5-fold-coordinated nickel.

However, the use of the Co and Ni sulfide structures as references supposes that the promoted Co(Ni)MoS catalysts consist of a heterogeneous mixture of Co sulfide and MoS_2, so the synergetic effect would be difficult to understand. Instead we discuss the incorporation of the promoter atoms in a homogeneous PMoS (P = promoter) phase.

B. Intercalation and Pseudointercalation Models

Bulk MoS_2 exhibits a layered structure in which van der Waals forces acting between two successive S–Mo–S sheets provide interlayer cohesion. The dispersion of the active phase on the carrier implies that only a few sheets are stacked together. The stacking number (which may depend on the activation process) has been shown experimentally to vary between 1 and 3 (38). Two MoS_2 layers at least are required to intercalate the promoter atoms. We suppose that one cobalt atom per molybdenum atom present on the molydenum edge is inserted in the van der Waals gap. The cobalt atoms are inserted on both sides of the slab as shown in Fig. 2. All calculations were performed for Co and the results are inferred to hold for Ni.

1. Energetics. The intercalation model proposed in Refs. (8, 9) and the pseudointercalation of Ref. (10) refer actually to a general problem: determining the potential energy surface (PES) of the promoter atom inside the van der Waals gap. Assuming that the promoter is localized in this region, its equilibrium position will be determined as the site where the potential energy reaches a minimum. We have not determined the full PES, but we have calculated the energy for four high-symmetry positions as starting configurations: the surface pseudointercalation (position (a)

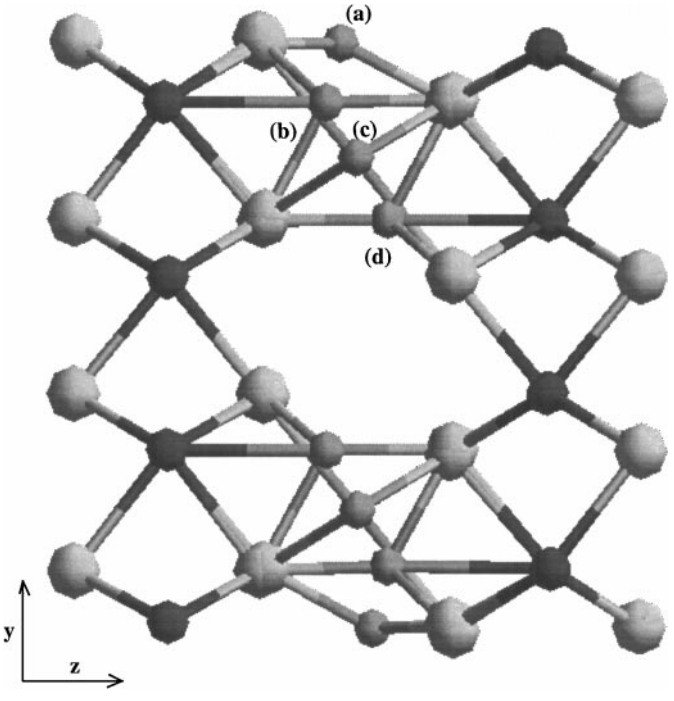

FIG. 2. Side view of the promoted MoS_2 slab for four different high-symmetry positions of the promoter atom: (a) surface pseudointercalation, (b) tetrahedral pseudointercalation, (c) octahedral pseudointercalation, and (d) bulk tetrahedral intercalation. Large light gray balls, S atoms; medium black balls, Mo atoms; small dark gray balls, Co atoms. (All bonds are drawn according to a geometrical criterion and should not be interpreted as being a chemical bonding.)

TABLE 2

Calculated Total Energies (eV/Cell) for the Intercalation Models and Edge Addition Models of the CoMoS System

Promoter location	Optimized structure	Total energy
surface pseudointercalation	Fig. 3(a)	−530.22
tetrahedral pseudointercalation	Fig. 3(b)	−536.13
octahedral pseudointercalation	Fig. 3(c)	−530.93
bulk tetrahedral intercalation	Fig. 3(d)	−533.62
addition on the S edge side	Fig. 3(e)	−529.92

Note. All the cells have the same compositions.

in Fig. 2), the tetrahedral pseudointercalation (b), the octahedral pseudointercalation (c), and the "bulk" intercalation (d).

For all models a complete relaxation via minimization of energy and forces is performed. In addition we have considered the possibility of adsorbing Co in a 4-fold-coordinated position on the S-terminated edge (Fig. 3(e)). Total energies calculated for the optimized structures are given in Table 2. From the total energy results we can rule out four cases: the surface pseudointercalation, the octahedral pseudointercalation, the bulk tetrahedral intercalation, and the edge addition. The most favorable position is the tetrahedral pseudointercalated position (position (b) in Fig. 2 or Fig. 3(b)), where the promoter is 4-fold coordinated by sulfur atoms and has one molybdenum neighbor.

2. Structural analysis. The optimized structures for all five models, together with the interatomic distances around the promoter atoms, are given in Figs. 3(a) to 3(e). The comparison with EXAFS data is given in Table 3.

We have to consider the optimized distances which are the most characteristic for the local environment of the promoter. The experimental Co–S and Co–Mo distances are the most relevant for the comparison with the calculated distances (the experimental and calculation accuracies are both within 0.05 Å).

TABLE 3

Comparison with EXAFS Data of the ab Initio Calculated Distances after Relaxation for the Various CoMoS Models

Model	d_{CoS} (Å)	N_{CoS}	d_{CoMo} (Å)	N_{CoMo}
EXAFS from Refs. (14, 15)	2.18–2.24	4.9–6.2	2.80–2.87	1.7–2.0
surface pseudo-intercalation	2.11–2.14	3.0	2.90	1.0
tetrahedral pseudo-intercalation	2.13–2.22	4.0	2.69	1.0
octahedral intercalation	2.22^a and 2.52^b	3.0^a and 3.0^b	>3.3	—
bulk tetrahedral intercalation	2.13–2.16	4.0	2.67	1.0
S edge substitution	2.32	6.0	2.95	2.0
Mo edge substitution	2.21	4.0	2.84	2.0

Note. The distance d^a (resp. d^b) corresponds to the coordination number N^a (resp. N^b).

The surface intercalation model (Fig. 3(a)) yields a slightly too short Co–S distance and a slightly too large Co–Mo distance. This confirms the energetic result which shows that evidently this site is energetically disfavored.

The starting configuration for the octahedral model was chosen with cobalt in the octahedral hole and Co–S distances between 2.36 and 2.43 Å. After relaxation (see Fig. 3c), the cobalt atom has been displaced along the *y*-direction closer to the surface so that there are only three short Co–S distances (about 2.22 Å) in a distorted octahedral environment. In this configuration, the shortest Co–Mo distance is 3.35 Å, clearly outside the range covered by the EXAFS data.

For the edge addition model, the calculated Co–S distance of 2.32 Å is too large and the Co–Mo distance of 2.27 Å is too short (see Fig. 3(e)). Even if we assume that the sulfur coordination of cobalt may be higher, the S–Mo distance would increase so that the discrepancy in the Co–S distance would be even larger. This confirms that this model is not acceptable either from the energetics or from the structural results.

Among the intercalation models, the tetrahedral pseudointercalation model (Fig. 3(b)) and the bulk tetrahedral intercalation (Fig. 3(d)) are energetically favored, but both exhibit slightly too short Co–S distances (between 2.13 and 2.22 Å) as well as too short Co–Mo distances (2.65 and 2.67 Å).

The EXAFS analysis also gives rough estimates of the CoS and CoMo coordination numbers ($N_{CoS} = 4.9$–6.6, $N_{CoMo} = 1.7$–2.0). Inspections of Figs. 3(a) to 3(d) clearly shows that all intercalation models predict consistently lower coordination numbers. The exception is for the octahedral model where the CoS coordination is 6, but here Co has no Mo neighbors. Hence, we conclude that, from a structural point of view, the intercalation and adatom models are not compatible with the EXAFS data.

C. Substitution Models

Within the decoration model, the promoter atom could also substitute for one of the molybdenum edge sites. On the metal edge, we first assume that the cobalt atoms replacing Mo are initially not saturated by adsorbed sulfur, so that the cobalt is tetracoordinated with sulfur (see Fig. 4(a)). On the S edge, we suppose in this section that the cobalt atoms substituting for the Mo atoms in the top bilayer are initially fully saturated by the sulfur edge atoms (see Fig. 4(b)). As a third case, exhibiting the same composition, we consider the substitution of molybdenum atoms in the deeper layers (bulk substitution in Fig. 4(c)).

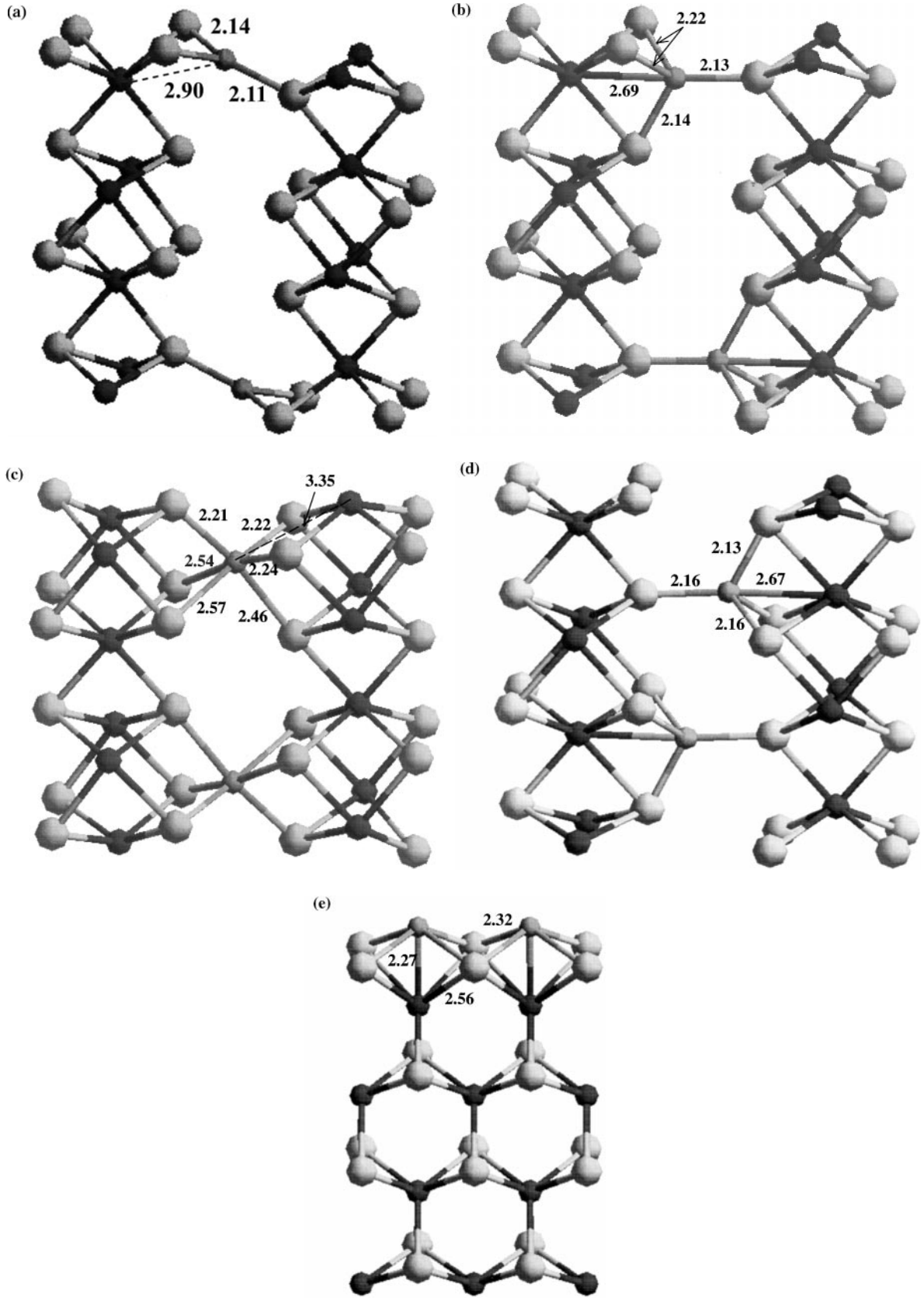

FIG. 3. Fully optimized structure for intercalation models: (a) surface pseudointercalation, (b) tetrahedral pseudointercalation, (c) octahedral pseudointercalation, (d) bulk tetrahedral intercalation, and (e) addition on the S-terminated edge. For the sake of clarity, a smaller cell than the one used for the calculation (see Fig. 1) is represented. (All distances are in angstroms.)

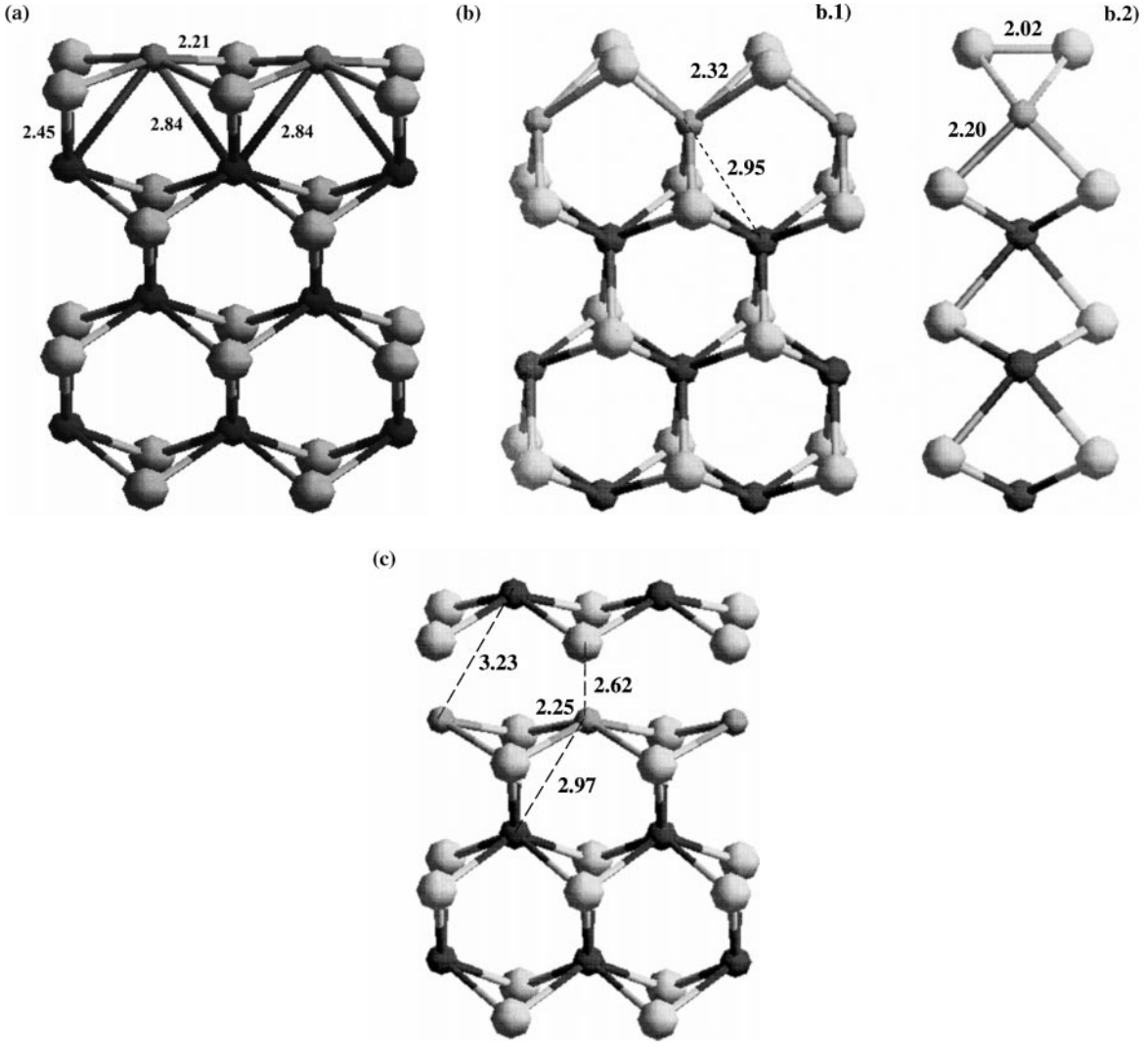

FIG. 4. Fully optimized structures for substitution models: (a) on the Mo edge, (b) on the S edge, and (c) in the bulk. For the sake of clarity, a smaller cell than the one used for the calculation (see Fig. 1) is represented. (All distances are in angstroms.)

1. Energetics. (a) Comparison of various substitution models. The total energies for the different configurations represented in Fig. 4 are given in Table 4. The bulk substitution is clearly ruled out. The explanation is that the trigonal prismatic environment is highly unfavorable for the cobalt atom. In previous work (21), we have investigated various experimental as well as hypothetical bulk structures for cobalt sulfides. This ab initio study has clearly pointed out the destabilization of the layered disulfide structure versus the pyrite structure for transition metal atoms belonging to columns 8, 9, and 10.

TABLE 4

Calculated Total Energies (eV/Cell) for Different Promoter Locations in the Substitution Model

Promoter localization	Optimized structure	Total energy (eV/cell)
substitution on the Mo edge side	Fig. 4(a)	−471.72
substitution on the S edge side	Fig. 4(b)	−461.56
bulk substitution	Fig. 4(c)	−455.70

Note. All the cells have the same compositions.

The substitution of Mo by Co atoms on the saturated S edge leads to the same conclusion, even if the destabilization of the structure is less strong in terms of the total energy, because of the surface relaxation.

The reason is the same as for the bulk substitution. If some cobalt atoms exist in a substitutional site on the S edge, strong reconstructions should occur on this plane. One possibility is that the coordination number of cobalt should be

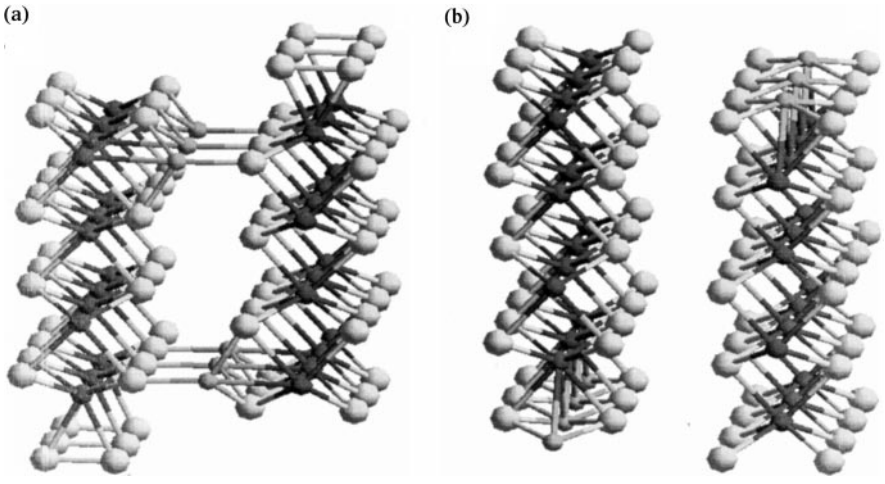

FIG. 5. Fully optimized structures for (a) the tetrahedral pseudointercalation and (b) the substitution on the Mo edge models. Both cells have the same composition. The cell for the substitution model contains four rows of MoS_6 prisms in the *y*-direction plus one Co row on each side of the slab.

lower to reach a more stable state offered by a tetrahedral environment (such as that found in Co_9S_8).

(b) Comparison with the tetrahedral pseudointercalation model. At this stage of the study we can compare the energetics of the two most stable models previously found: the tetrahedral pseudointercalation model (see previous section) and the model with substitution of Mo by Co atoms on the Mo edge.

Nevertheless, for such a comparative calculation, both cells have to exhibit the same amounts of S, Mo, and Co atoms as represented in Figs. 5(a) and 5(b). The cell describing the substitution model is larger than the one used previously: four rows of MoS_6 prisms in the *y*-direction (plus one row of Co atoms on each side of the slab). We have carefully tested (see also Ref. (27)) and verified that the influence of the slab thickness is negligible when more than four rows of MoS_6 prisms are considered. The structural analysis (presented in the next paragraph) reveals that no significant differences are observed whether four or five rows of metals are considered. After a full relaxation of both cells, the total energy values show that the substitution of Mo by Co (Fig. 5(b)) is stabilized by about 1.7 eV per cell in comparison with the pseudointercalation model (Fig. 5(a)). This result provides us with a strong argument for a preferential localization of the promoter atoms on the edge and substituting the Mo atoms.

2. Structural analysis. In the case of a substitution of Mo by Co in a subsurface layer, relaxation effects lead to an inward displacement of the plane containing cobalt and thus an increase of the distance between the subsurface layer and the outer MoS_2 layer (see Fig. 4(c)). The distance between the substituted Co atom and the S atoms increases to 2.62 Å. This shows that bulk substitution is incompatible with the EXAFS results. Furthermore, the weak bonding of the surface layer to the bulk explains why bulk substitution is energetically unfavorable.

The substitution of Co for Mo in the top layer of the S edge (see Fig. 4(b)) leads to a weak bonding of the surface S atom (so that the Co–S bond is slightly too long). However, a definitely unrealistic aspect of this model is the formation of a strong S–S bond with a bond length of only 2.02 Å.

The substitution of the molybdenum located on the Mo edge leads after relaxation to the configuration represented in Fig. 4(a). The comparison of the calculated Co–S and Co–Mo distances with the EXAFS data is given in Table 3. In agreement with Ref. (14), we observe immediately on the edge a slight inward relaxation of the cobalt atom because the surface Co–S distances (2.21 Å) are about 0.2 Å shorter than the Mo–S distances. The calculated Co–Mo distances are about 2.84 Å. This model exhibits clearly the best agreement with EXAFS data, apart from a slightly underestimated Co–S coordination (but remember that the EXAFS data do not exclude a partial sulfidation of the Mo edge).

We have also investigated the possibility of an only partial substitution of Mo by Co on the Mo edge. The degree of substitution is expressed in terms of the atomic ratio Co/M_S, where M_S stands for the number of surface metal sites of the Mo edge.The optimized configurations for Co/M_S ratios of 0.33 and 0.66 are shown in Figs. 6(a) and 6(b). The important point to note is that the substitution of Mo by Co is a very local process: the Co–S and Co–Mo distances are almost the same if the substituted Co atoms have only Mo neighbors on the edge, or have one Co and one Mo neighbor, or form a continuous Co edge.

At this stage of the study, the best model from the energetic and structural points of view is the substitution of the molybdenum atoms located on the Mo edge by a promoter atom (here Co). The substitution of the molybdenum

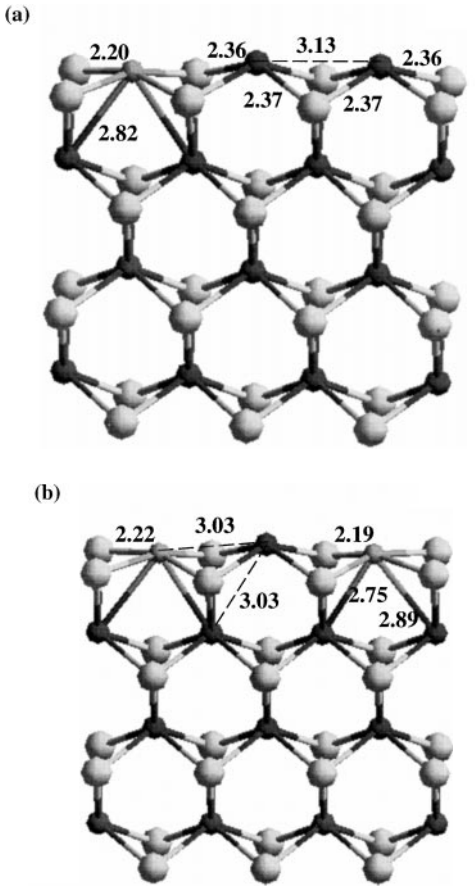

FIG. 6. Fully optimized structures for the substitution models on the Mo edge side with various Co surface contents: (a) $Co/M_S = 0.33$ and (b) $Co/M_S = 0.66$. (All distances are in angstroms.)

sites located on the S edge has to be further investigated by modifying the sulfur coverage. This is the scope of the next section, which also continues our previous work on S adsorption/desorption on the unpromoted MoS_2 catalyst (27).

D. Effects of the Promoters on the Surface Sulfur Coverage in a Sulfiding Environment

1. S-terminated edge. (a) Energetics. Here we calculate the energetic cost of removing one S atom (corresponding to 17% coverage) from the S edge on which the top row of Mo atoms has been replaced by Co. We consider the reaction

$$(\mathrm{CoMoS}) + \mathrm{H_2} \Leftrightarrow (\mathrm{CoMoS} + \mathrm{vacancy}) + \mathrm{H_2S}. \quad [1]$$

The reaction enthalpy is given in Fig. 7. The reference energy is that of the optimized configuration shown in Fig. 4(b). We find that the removal of up to three S atoms (50% S coverage) is an exothermal process, in contrast to unpromoted MoS_2, where we found endothermal heats of reaction when we desorbed up to 50% S atoms (27).

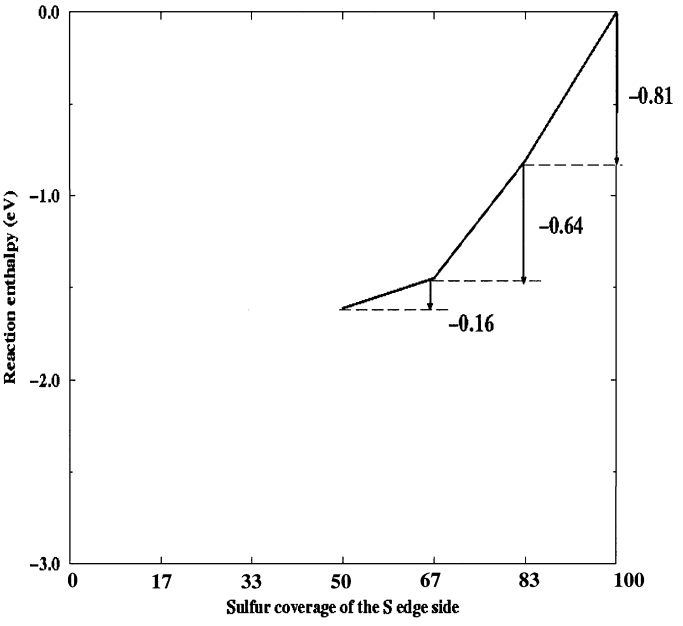

FIG. 7. Variation of the reaction enthalpy ΔE (in electronvolts) for the creation of sulfur vacancies as a function of the sulfur coverage (in percent) of the S edge of the promoted catalyst ($Co/M_S = 1$). The fully saturated surface is the energy reference.

(b) Structural analysis. For the 50% S coverage, the cobalt atoms are in a tetrahedral environment and the local structure is shown in Fig. 8. The symmetric chain-like arrangement of the top S atoms was not found on the nonpromoted system. The optimized Co–S and Co–Mo distances on the S-depleted edge compare better with the EXAFS data (see Table 5) than in the case of a 6-fold-coordinated Co atom placed in trigonal prismatic environment (Table 3). Nevertheless, the Co–S distances appear to be slightly underestimated whereas the Co–Mo distance would be slightly overestimated.

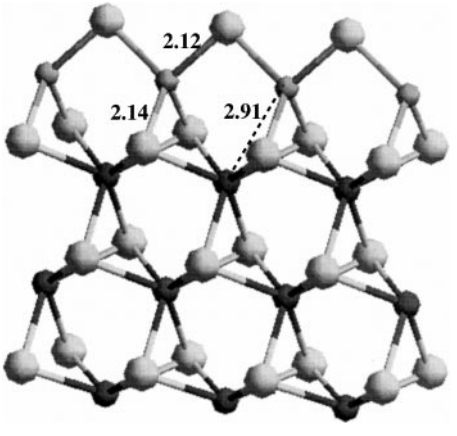

FIG. 8. Fully optimized structure of the S edge of the Co-promoted MoS_2 for $Co/M_S = 1$ with a sulfur coverage of 50%. (All distances are in angstroms.)

TABLE 5

Ab Initio Calculated Distances for the Substitution Models for the Two Edges and Different Coordination Numbers of Co

Edge side	N_{CoS}	d_{CoS} (Å)	N_{CoMo}	d_{CoMo} (Å)
S edge	6.0	2.31	2.0	2.95
S edge	4.0	2.11–2.14	2.0	2.91
Mo edge	4.0	2.20–2.22	2.0	2.79–2.84
Mo edge	5.0	2.17–2.24	2.0	2.87–3.00
Mo edge	6.0	2.23–2.26	2.0	2.92–2.98

2. Mo-terminated edge. (a) Energetics. On the Mo-terminated edge, we have considered the adsorption of S atoms on the Mo(Co) sites according to the reaction

$$CoMoS + nH_2S \Leftrightarrow (CoMoS + nS) + nH_2 \qquad [2]$$

for different values of the degree of substitution expressed in terms of the fraction of Co atoms on the metal edge sites (M_S). Fig. 9 shows the calculated reaction enthalpies versus the sulfur coverage of the metal (CoMo) edge for different degrees of substitution varying from $Co/M_S = 0$ to $Co/M_S = 1$. We find that, like for the unpromoted MoS_2 catalyst, adsorption of S on the coordinatively unsaturated metal sites is an exothermal process up to a S coverage of one S per surface metal atom (corresponding to 50% of the maximum coverage for unpromoted MoS_2). However, we find that the reaction enthalpies decrease strongly with increasing Co/M_S ratio—for a fully substituted metal edge, the adsorption energy for a single sulfur atom is only 0.04 eV/atom (0.6 kcal/mol), and the adsorption of more S atoms is even slightly endothermic. A similar conclusion holds for partial Co for Mo substitution: the first S adsorption is moderately exothermic, but further S adsorption leads to only weakly bound S atoms. The equilibrium concentration of S adsorbed on the metal edge could be analyzed in detail using the same formalism as used for the unpromoted MoS_2 (27). However, we already see from the reaction enthalpies plotted in Fig. 9 that, under usual HDS conditions, the S coverage of the promoted CoMoS will be around 17%, in contrast to the unpromoted catalyst, where we found 50% S coverage over a wide range of sulfiding conditions.

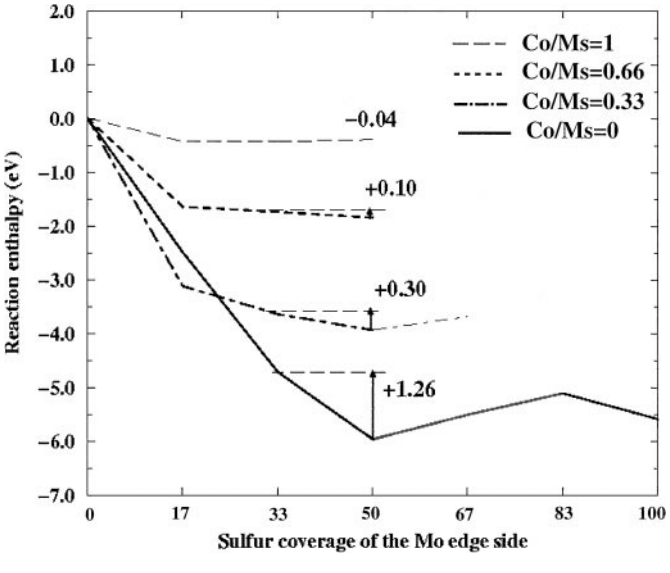

FIG. 9. Variation of the reaction enthalpy ΔE (in electronvolts) for sulfur adsorption as a function of the sulfur coverage of the Mo edge of the promoted catalyst with various cobalt contents. The bare surface is the energy reference.

(b) S coverage under varying chemical potentials. In the same spirit as in our previous work on the nonpromoted system (27), we plot in Fig. 10(a) the grand potential, Ω, of the metal-terminated edge as a function of the chemical potential of sulfur in the gas phase. In Fig. 10(b) we have reproduced the diagram for the nonpromoted systems. The chemical potential of S is expressed as a function of the ratio of the partial pressures of H_2S and H_2 and of temperature. For the typical working conditions ($P_{H_2S}/P_{H_2} = 0.01$ and $T = 650$ K), the chemical potential is located around −1 eV (refered to bulk sulfur deposition, see Ref. (27) for more details). In comparison with the nonpromoted system (see Fig. 10(b)), we observe that the main effect of the promoter is to decrease the equilibrium sulfur coverage from 50% to values between 0 and 17% for $Co/M_S = 1$. For intermediate Co/M_S ratios, intermediate equilibrium sulfur coverages are reached.

We must be aware of the fact that the effect of hydrogen adsorbed on the surface is not considered here. For high S content on Co-promoted systems with $Co/M_S = 1$, our simulations reveal that S dimers may exist on the metal edge. Nevertheless, such S dimers should not be present if surface–SH groups are present avoiding S–S interactions. We are currently studying the influence of adsorbed H species. Nevertheless, the trends revealed for the sulfur chemical potential corresponding to working conditions should essentially not be changed with the Co-promoted system, exhibiting low sulfur coverage.

(c) Structural analysis. Figure 11 presents the most stable configurations for various sulfur coverages and Co/M_S ratios. For complete substitution of Mo by Co and sulfur coverage between 17% and 50%, the most stable adsorption site for sulfur is a bridging position between two Co atoms. The Co–S distances of the adsorbed S atoms are slightly shorter than those of the S surface atoms. S adsorption increases also the Co–Mo distances. Hence, S adsorption leads to interatomic distances which are still in acceptable agreement with EXAFS results and even slightly improves the agreement for the Co–S coordination numbers.

Figures 11(a) to 11(e) show the optimized geometries for S adsorbed on a partially Mo/Co-exchanged metal edge.

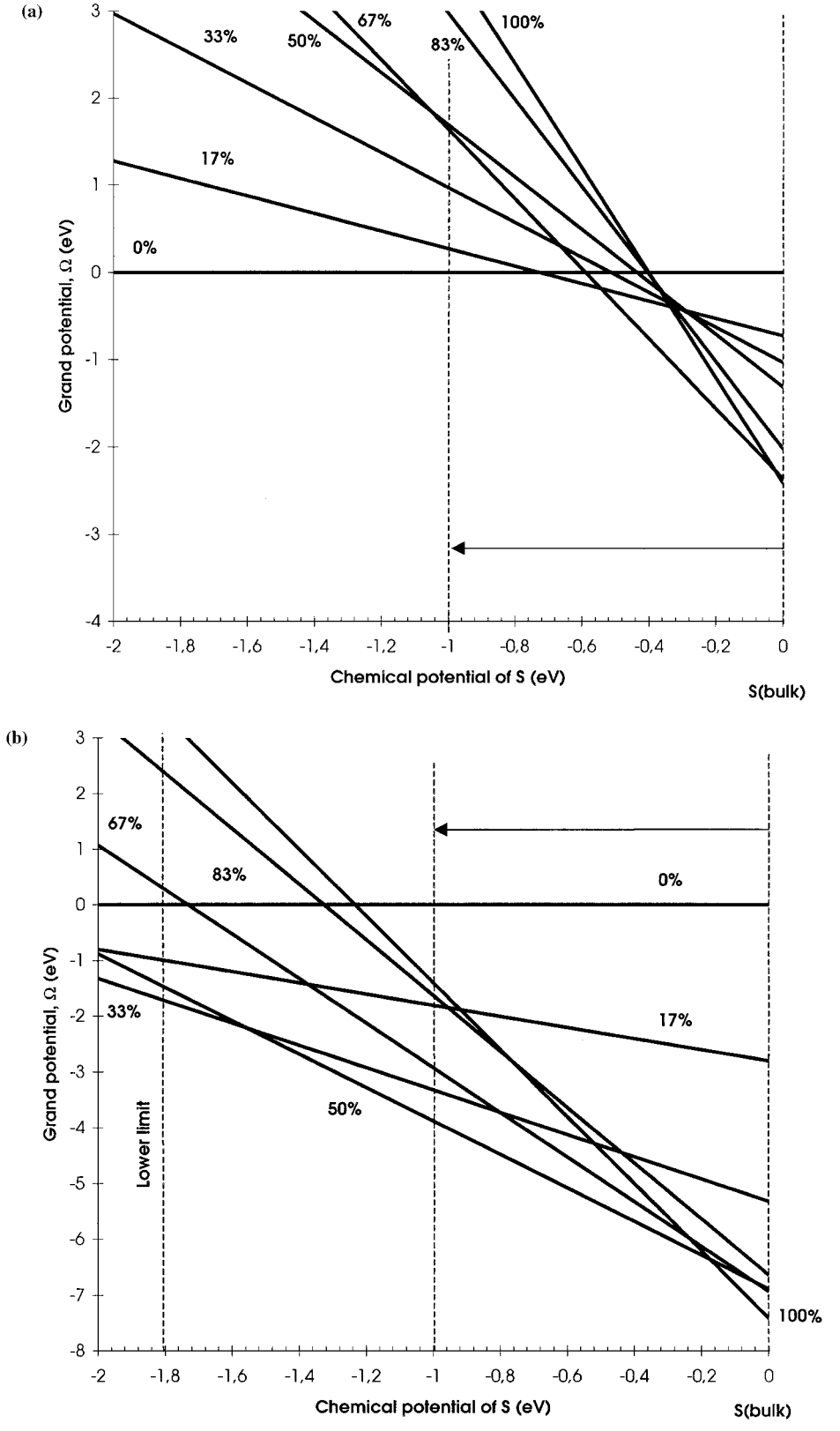

FIG. 10. Grand potential, Ω (in electronvolts), as a function of the chemical potential of S on the metal edge for the Co-promoted system ($Co/M_S = 1$) (a) and for the nonpromoted MoS_2 from Ref. (27) (b). Each line corresponds to a given sulfur coverage. The energy references for μ_S are the crystalline α phase of S and the stoichiometric as-cleaved surface for the surface formation energy. The arrow represents an estimation of μ_S for the experimental conditions ($T = 650$ K and $P_{H2S}/P_{H2} = 0.01$; for more details see also Ref. (27)).

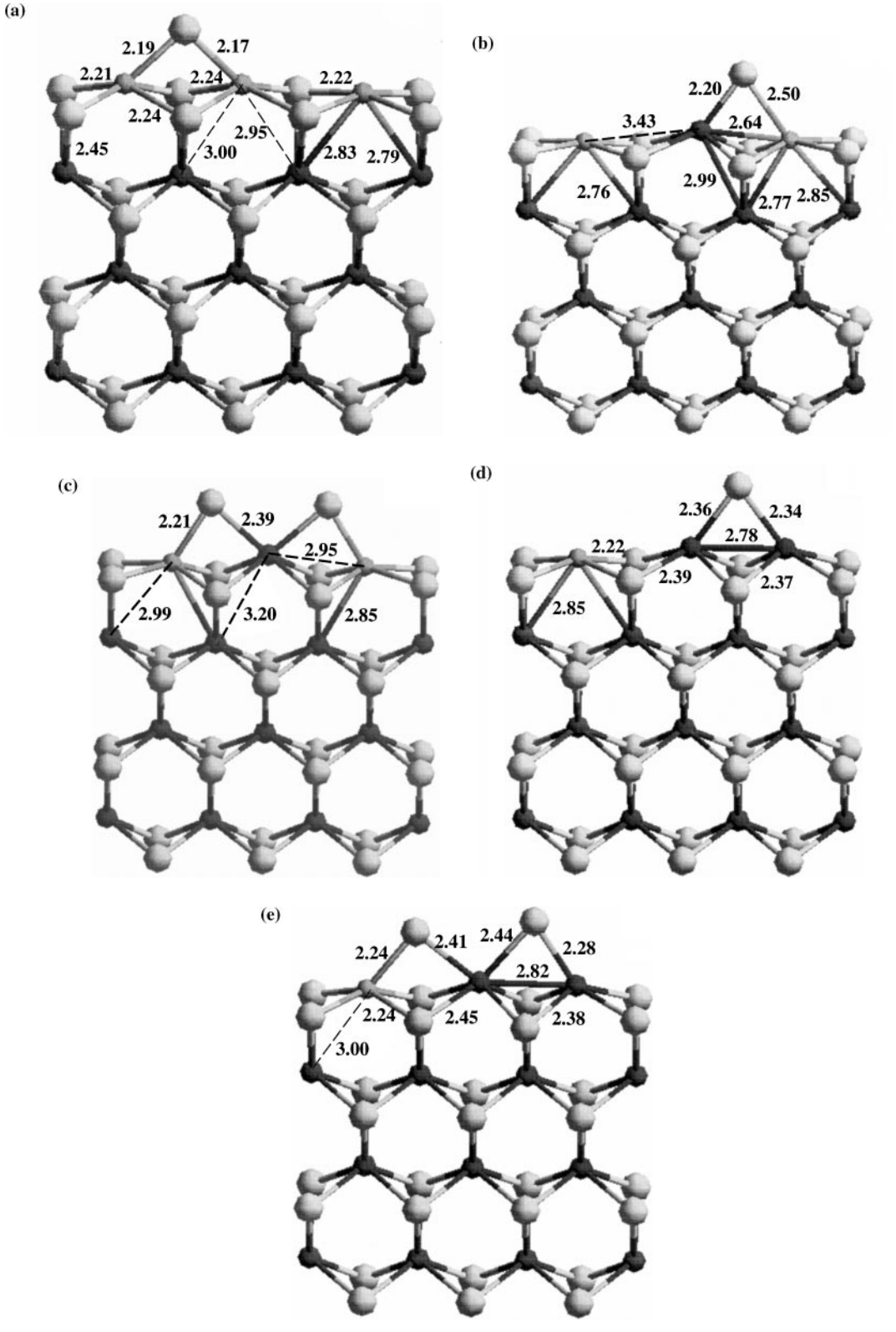

FIG. 11. Fully optimized structures of the promoted Mo edge with various cobalt contents and various sulfur coverages: (a) $Co/M_S = 1$ and 17% S, (b) $Co/M_S = 0.66$ and 17% S, (c) $Co/M_S = 0.66$ and 33% S, (d) $Co/M_S = 0.33$ and 17% S, and (e) $Co/M_S = 0.33$ and 33% S. (All distances are in angstroms.)

TABLE 6

Comparison of the Local Structure with Electronic Properties and for $PT/M_S = 1$ for the Bare Surface (0% S)

Metal atom (M)	M–S (Å)	M–Mo (Å)	d_{yz} orbital[a]
Mo	2.37	3.11	+0.53
Co	2.21	2.84	−0.33
Ni	2.17	2.75	−0.63
Cu	2.21	2.86	<−1

[a] Position in electronvolts with respect to the Fermi level.

In the presence of a coordinatively unsaturated Mo atom, S always binds preferentially to the Mo site, in a bridging position either between one Co and one Mo atom or between two Mo atoms. Co–S distances are shorter than Mo–S distances ($d_{CoS} \simeq 2.20$–2.24 Å, $d_{MoS} \simeq 2.34$–2.40 Å); the exception is the case of an isolated S atom on a surface with $Co/M_S = 0.66$. In this case the Mo–S distance is shorter, because the 5-fold-coordinated Mo atom is still coordinatively unsaturated. The distances between Mo and adsorbed S are shorter than the Mo–S distances in the bulk. Co–Mo and Mo–Mo distances between the surface and the subsurface are slightly elongated by S adsorption, but at low S coverage (i.e., in the physically realistic range) the calculated Co–Mo distances (as well as the Co–S distances) remain within the range covered by the EXAFS data.

E. Case of Ni- and Cu-Promoted Systems

We now substitute a Mo atom located on the Mo-terminated edge by Ni or Cu. From the structural point of view, no significant changes are observed (see Table 6). As for the energetics, we observe that the sulfur–metal bond energy is significantly lower for NiMoS with $Ni/M_S = 1$ than for the CoMoS with $Co/M_S = 1$ (see Table 7). For the CuMoS system with $Cu/M_S = 1$, the energy required for desorbing one sulfur atom on the CuMo-terminated edge is even lower. So the sulfur coverage at equilibrium will be displaced toward a very small value (below 17%) and this displacement is higher in the case of Ni than for Co, and even higher for Cu than for Ni. The very high endothermicity for the sulfur adsorption on the CuMoS system will be proposed in the discussion as an explanation for the nonpromoting effect of Cu.

TABLE 7

Sulfur Metal–Bond Energy at the Estimated Sulfur Coverage Equilibrium for Various Surface Cobalt Contents

PT	PT/M_S	Sulfur coverage	ΔE (eV)
—	0	0.50	+1.26
Co	0.33	0.33–0.50	+0.30 to +0.52
Co	0.66	0.17–0.33	+0.10
Co	1	0.17	+0.00
Ni	1	<0.17	−0.41
Cu	1	<0.17	−1.17

F. Electronic properties. The electronic properties of the Mo edge and S edge surfaces of the nonpromoted catalyst have been studied in detail in Refs. (25–27). The unoccupied surface states just above the Fermi level have d_{yz} and $d_{x^2-y^2}$ symmetries (if y is the direction perpendicular to the surface and z the direction perpendicular to the basal plane). The acceptor role of these orbitals and in particular of the d_{yz} orbitals for a π electron donor molecule such as thiophene was proven in Ref. (26). Once a promoter atom (cobalt or nickel) has been substituted for a molybdenum on an edge site, the local density of states (DOS) projected on the promoter atom is given by Fig. 12. In Figs. 12a to 12c we analyze the change of the local DOS at the substituted Co atoms as a function of the Co/M_S ratio and for the equilibrium sulfur coverage. We also differenciate between 4- and 5-fold-coordinated sites for $Co/M_S = 1$. The most important effect is the shift of the d_{yz} below the Fermi level. This displacement is slightly larger for 5-fold-coordinated sites (i.e., with a S atom bound to the Co site; see Figs. 12(c) and 12(d)). It increases with the Co/M_S ratio.

Figures 13(a) to 13(c) analyze the change of the local DOS at the Mo sites as a function of the Co/M_S ratio. For the unpromoted Mo edge (Figs. 13(a) and 13(b)), we find that the high local DOS of the bare surface (and therefore the high reactivity of the coordinatively unsaturated Mo sites) is strongly reduced with increasing sulfur coverage and Mo–S coordination: the electron transfer to the adsorbed S atoms depletes the Mo d states at the Fermi level. With increasing Co/M_S ratio (Figs. 14(c) and 14(d)), this trend becomes even more pronounced: for partially or completely S-saturated Mo sites, even a surface gap or pseudogap is formed just above the Fermi level.

The change of the local S DOS as a consequence of the Co/Mo substitution is analyzed in Fig. 14. For unpromoted MoS_2 and an equilibrium S coverage of 50%, we find only a very low S DOS at the Fermi level and this is not changed at Co/M_S ratios up to 0.66. Only at a complete Co/Mo substitution do unsaturated S states appear at the Fermi level.

The positions of the d_{yz} state at Mo sites in unpromoted MoS_2 and at Co or Ni in promoted CoMoS or NiMoS catalysts are summarized in Table 6. The shift is larger for nickel than for cobalt according to a higher degree of d band filling. The $d_{x^2-y^2}$ orbitals remain above the Fermi level but the unoccupied d_{yz} states are now fully filled by the cobalt (or nickel) d electrons. The local DOS at the Ni sites of the fully substituted Mo edge is shown in Fig. 15, demonstrating a strongly reduced local DOS at the Fermi level compared to that of the fully substituted CoMoS. For copper, the trend is further followed. The shift in the position of the d_{yz} state paralles the change in the heat of

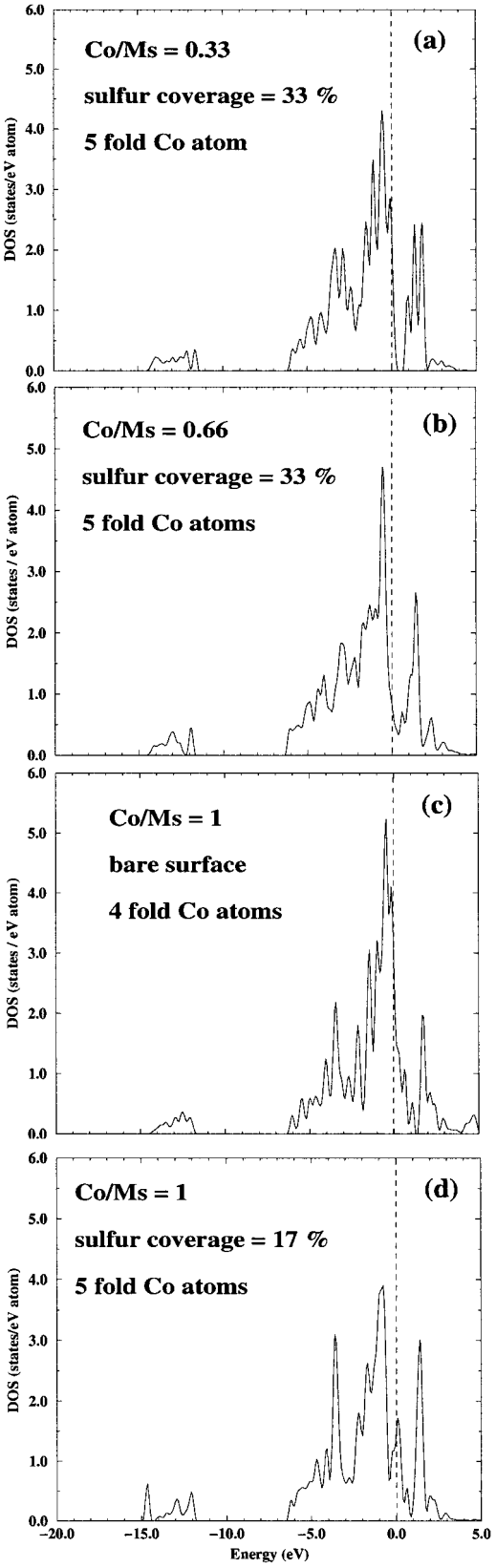

FIG. 12. Local densities of states projected on the Co sites of the promoted surface: (a) $Co/M_S = 0.33$ and 33% S, (b) $Co/M_S = 0.66$ and 33% S, (c) $Co/M_S = 1$ and 0% S, and (d) $Co/M_S = 1$ and 17% S.

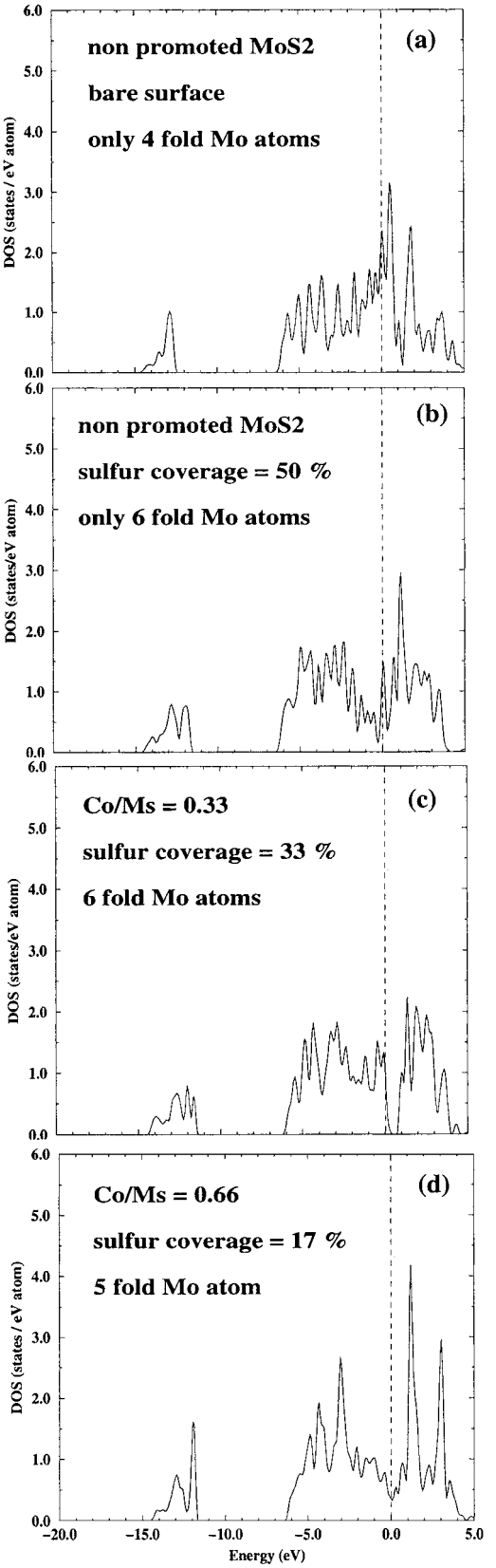

FIG. 13. Local densities of states projected on the Mo sites: (a) nonpromoted MoS_2 and 0% S, (b) nonpromoted MoS_2 and 50% S, (c) $Co/M_S = 0.33$ and 33% S, and (d) $Co/M_S = 0.66$ and 17% S.

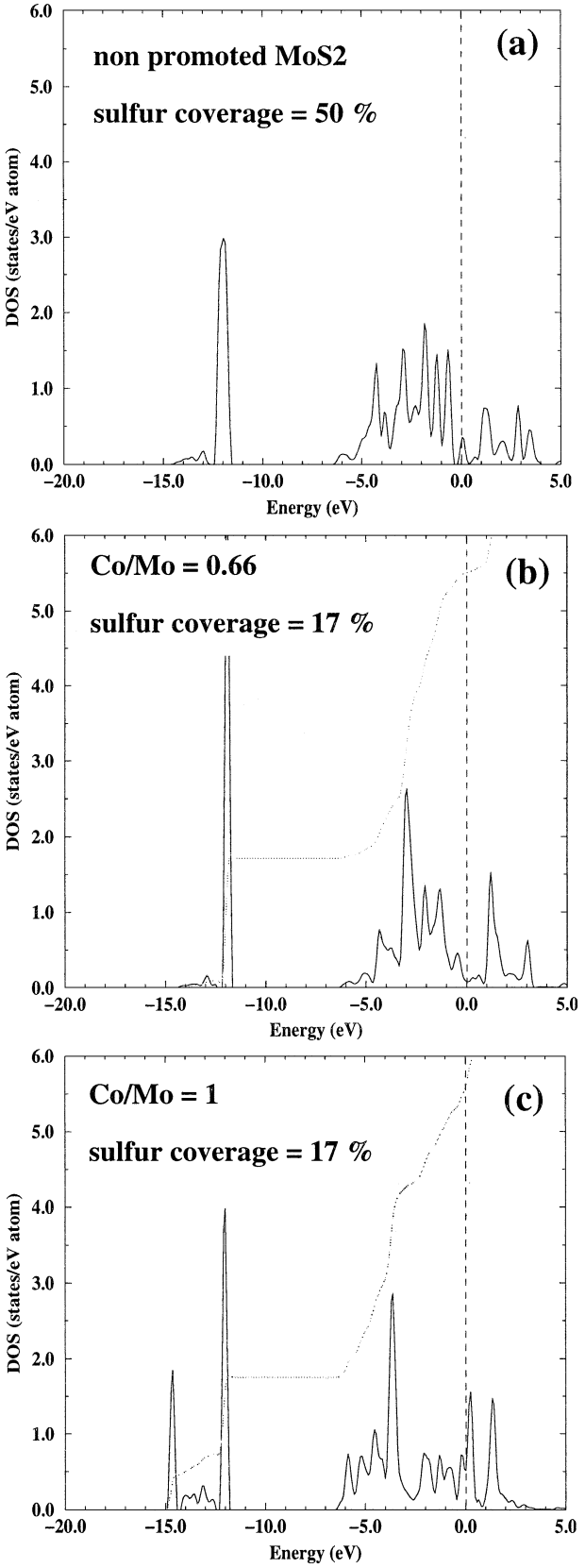

FIG. 14. Local densities of states projected on the S sites: (a) non-promoted MoS_2 and 50% S, (b) $Co/M_S = 0.66$ and 17% S, and (c) $Co/M_S = 0.33$ and 17% S.

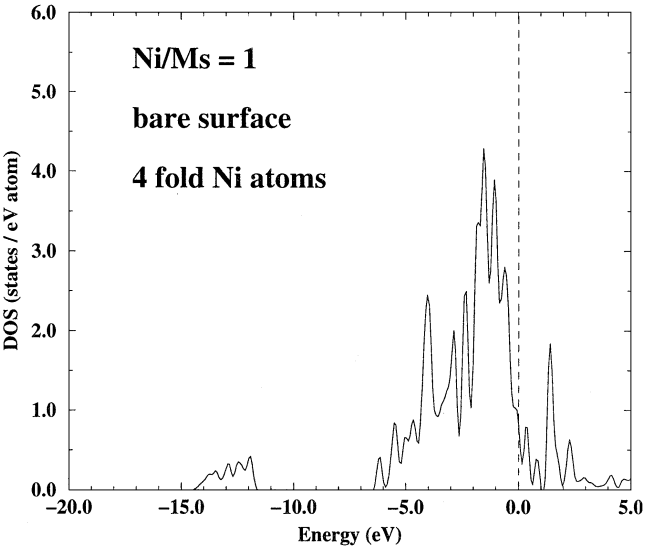

FIG. 15. Local density of states projected on the Ni sites of promoted NiMoS ($Ni/M_S = 1$).

adsorption of S (calculated according to the reaction [2] used above). On the Ni-promoted surface even the first adsorption step is exothermic, continuing the trend from unpromoted MoS_2 to CoMoS discussed above (see Table 6). Cu-promoted MoS_2 goes even further in this direction.

IV. DISCUSSION AND CONCLUSIONS

The most favorable localization of the promoter (Co or Ni) is found for the substitution of the Mo atoms by Co (or Ni) atoms located at the edges. The tetrahedral pseudointercalation is less favored for structural and energetic reasons. Nevertheless, we cannot definitively exclude that it might take place for high Co (or Ni) contents once all Mo sites at the edges are substituted by the promoter atoms. The pseudointercalation has been interpreted to occur from HREM observations of bulk crystalline MoS_2 for high Co loading (11). But for real dispersed catalysts a few nanometers in size and with stacking numbers around 2, it is impossible to account for the well-known occurrence of a maximum in HDS activities for a $Co/(Co + Mo)$ ratio close to 0.3 with a pseudointercalation model. Indeed, the geometrical model (12) shows that one promoter atom per Mo edge atom is mandatory to account for this ratio. With a pseudointercalation model, two Mo edge atoms for one promoter atom are required for an average stacking number of 2, which leads to a $Co/(Co + Mo)$ ratio at the optimum significantly lower than 0.3.

The study of the variation of the structure of promoted CoMoS at different S coverages confirms that the substitution model on the edges is best compatible with the EXAFS data. Nevertheless, two cases have to be distinguished: the substitutions of a molybdenum site on the Mo-terminated edge and on the S-terminated edge.

On the S edge, removal of up to 50% of S atoms is now an exothermic process, in contrast to that on unpromoted MoS_2, where it is strongly endothermic. For the fully Co-exchanged edge with an equilibrium S coverage of 50%, the calculated interatomic distances remain compatible with the EXAFS studies.

On the Mo edge, the exothermic heat of reaction for S adsorption is progressively reduced with increasing Co/M_S ratio. Adsorption of more than one S atom on our model (i.e., a coverage exceeding 17%) either is unfavorable (at a high Co content) or leads only to a weakly bound state. The calculated interatomic distances compare favorably with EXAFS results (Co–Mo distances) only for these low S coverages. This means that energetic considerations and EXAFS analysis lead to consistent results.

The evidence for a strong reduction of metal–sulfur bonding is already an important step toward understanding the promoter effect. The probability of deactivation of an active site by S adsorption is much lower on the promoted CoMoS than on the unpromoted MoS_2 catalyst.

We can compare this result with previous ab initio calculations on bulk sulfides (21, 22), where we found the following trend for the bulk sulfur metal bond energies:

$$MoS_2 \gg Co_9S_8 > Ni_3S_2$$

The decrease of the sulfur–metal bond energy by Co and Ni (as well as Cu) substitution is clearly confirmed on the surface.

Furthermore, we have shown that the higher the surface cobalt content, the lower is the sulfur–metal bond strength at the surface. The comparison between nickel, cobalt, and copper reveals that the Ni-promoted catalyst exhibits a weaker surface sulfur–metal bond than the Co-promoted catalyst. Cu would lead to an even weaker bond. Simultaneously, the equilibrium sulfur coverage is displaced toward very low values by increasing the cobalt content of the Mo edge plane. For an intermediate promoter content, the sulfur coverage (as well as the sulfur–metal bond energy) is intermediate so that once sulfur atoms are present on the surface, other sulfur compounds can be co-adsorbed. A full substitution of the molybdenum atoms by nickel atoms implies that the surface sulfur coverage should be lower than 17% since the removal of 17% of the sulfurs from this stage is exothermal.

We have found the following trends for the surface sulfur–metal bond energy at equilibrium (the index numbers correspond to the Co/M_S ratio, standing for the promoter content on the Mo edge surface, i.e., we quote surface stoichiometries):

$$MoS_2 > Co_{0.33}Mo_{0.67}S_2 > Co_{0.66}Mo_{0.33}S_2 > Co_1Mo_0S_2 > Ni_1Mo_0S_2 > Cu_1Mo_0S_2.$$

This trend is explained at an electronic level by the variation of the acceptor property of the surface correlated to the position of d_{yz} orbitals with respect to the Fermi level energy.

The exothermicity for the surface sulfur removal step calculated for $Ni_1Mo_0S_2$ and $Cu_1Mo_0S_2$ catalysts and the very low energy cost for the sulfur removal on $Co_1Mo_0S_2$ also suggest that the surface promoter content on the Mo edge should be optimized to enable a non-negligeable amount of adsorbed sulfur species. For too high PT/M_S atomic ratios, the quantity of sulfur compounds (Mo–S, Mo–SH, sulfur organic compounds) should be very low and would reduce the probability that a reaction occurs. In the same way, we explain the poisoning effect of copper suggested by Chianelli and Harris in HDS of DBT on Cu-promoted MoS_2 (20). Similarly, Wambeke *et al.* (39) detected no promoting effect of copper in the toluene hydrogenation reaction. The endothermicity of the sulfur adsorption is so high in this case that it indicates that the Mo edge surface is passivated by copper. This passivation may prevent the adsorption of S-bearing species or of aromatic hydrocarbons.

As the sulfur–metal bond energy seems to play a key role at the surface, we intend to pursue this work in the near future by establishing energy profiles for the full HDS mechanism. We have already undertaken such simulations for unpromoted MoS_2 (40), so we are confident that it will be possible to simulate the HDS mechanism for various surface promoter contents.

ACKNOWLEDGMENTS

This work has been performed within the Groupement de Recherche Européen "Dynamique Moléculaire Quantique Appliquée à la Catalyse," a joint project of the Conseil National de la Recherche Scientifique (CNRS), Institut Français du Pétrole (IFP), TOTALFINA, Universität Wien, and Schuit Institute of Catalysis. Work at Universität Wien has been supported by Institut Français du Pétrole (IFP) and by the Bundesministerium für Wissenschaft und Verkehr through the Center for Computational Materials Science (CMS).

REFERENCES

1. Grange, P., *Catal. Rev. Sci. Eng.* **21**, 135 (1980).
2. Clausen, B. S., Morup, S., Topsoe, H., and Candia, R., *J. Phys.* **37**, C6-249 (1976).
3. Wivel, C., Candia, R., Clausen, B. S., Morup, S., Topsoe, H., *J. Catal.* **68**, 453 (1981).
4. Chianelli, R. R., Ruppert, A. F., Behal, S. K., Kear, B. H., Wold, A., and Kershaw, R., *J. Catal.* **92**, 56 (1985).
5. Houssenbay, S., Kasztelan, S., Toulhoat, H., Bonnelle, J. P., and Grimblot, J., *J. Phys. Chem.* **93**, 7176 (1989).
6. Garreau, F. B., Toulhoat, H., Kasztelan, S., and Paulus, R., *Polyhedron* **5**, 211 (1986).
7. Kasztelan, S., Grimblot, J., and Bonnelle, J. P., *J. Phys. Chem.* **91**, 1503 (1987).
8. Voorhoeve, R. J. H., and Stuiver, J. C. M., *J. Catal.* **23**, 228 (1971).
9. Voorhoeve, R. J. H., *J. Catal.* **23**, 236 (1971).
10. Farragher, A. L., Cossee, P., *in* "Proceedings, 5th International Congress on Catalysis, Palm Beach, 1972" (J. W. Hightower, Ed.) p. 1301. North Holland, Amsterdam, 1973.
11. Chianelli, R. R., Ruppert, A. F., Jose-Yacamán, M., and Vázquez-Zavala, A., *Catal. Today* **23**, 269 (1995).

12. Kasztelan, S., Toulhoat, H., Grimblot, J., and Bonnelle, J. P., *Appl. Catal.* **13**, 127 (1984).
13. Topsoe, N-Y., and Topsoe, H., *J. Catal.* **84**, 386 (1983).
14. Bouwens, S. M. A. M., van Veen, J. A. R., Koningsberg, D. C., de Beer, V. H. J., and Prins, R., *J. Phys. Chem*. **95**, 123 (1991).
15. Topsoe, H., Clausen, B. S., Topsoe, N.-Y., Pedersen, E., Niemann, W., Müller, A., Bögge, H., and Lengeler, B., *J. Chem. Soc., Faraday Tran. 1* **83**, 2157 (1987).
16. Louwers, S. P. A., and Prins, R., *J. Catal.* **133**, 94 (1992).
17. Niemann, W., Clausen, B. S., and Topsoe, H., *Catal. Lett.* **4**, 355 (1990).
18. Bouwens, S. M. A. M., Koningsberg, D. C., de Beer, V. H. J., Louwers, S. P. A., and Prins, R., *Catal. Lett.* **5**, 273 (1990).
19. Harris, S., and Chianelli, R. R., *J. Catal.* **86**, 400 (1984).
20. Harris, S., and Chianelli, R. R., *J. Catal.* **98**, 17 (1986).
21. Raybaud, P., Hafner, J., Kresse, G., and Toulhoat, H., *J. Phys.: Condens. Matter* **9**, 11085 (1997); *J. Phys.: Condens. Matter* **9**, 11107 (1997).
22. Toulhoat, H., Raybaud, P., Kasztelan, S., Kresse, G., and Hafner, J., *Catal. Today* **50**, 629 (1999).
23. Byskov, L. S., Hammer, B., Norskov, J. K., Clausen, B. S., and Topsoe, H., *Catal. Lett.* **47**, 177 (1997).
24. Byskov, L. S., Norskov, J. K., Clausen, B. S., and Topsoe, H., *Prepr. Symp., Div. Petrol. Chem., Am. Chem. Soc.* **12** (1998).
25. Raybaud, P., Hafner, J., Kresse, G., and Toulhoat, H., *Surf. Sci.* **407**, 237 (1998).
26. Raybaud, P., Hafner, J., Kresse, G., and Toulhoat, H., *Phys. Rev. Lett.* **80**, 1481 (1998).
27. Raybaud, P., Hafner, J., Kresse, G., Kasztelan, S., and Toulhoat, H., *J. Catal.* **189**, 128 (2000).
28. Perdew, J. P., and Zunger, A., *Phys. Rev. B* **23**, 5084 (1987).
29. Perdew, J. P., Chevary, J. A., Vosko, S. H., Jackson, K. A., Pedersen, M. R., Singh, D. J., and Frolhais, C., *Phys. Rev. B* **46**, 6671 (1992).
30. Vanderbilt, D., *Phys. Rev.* **41**, 7892 (1990).
31. Kresse, G., and Hafner, J., *J. Phys.: Condens. Matter* **6**, 8245 (1994).
32. Kresse, G., and Hafner, J., *Phys. Rev. B* **47**, (1994), 588; *Phys. Rev. B* **49**, 14251 (1994).
33. Kresse, G., and Hafner, J., *Phys. Rev. B* **47**, 588, 14251 (1993).
34. Kresse, G., and Furthmüller, J., *Comput. Mater. Sci.* **6**, 15 (1996); *Phys. Rev. B* **54**, 11961 (1996).
35. Moroni, E., Kresse, G., Hafner, J., and Furthmüller, J., *Phys. Rev. B* **56**, 15629 (1997).
36. Bouwens, S. M. A. M., Koningsberg, D. C., de Beer, V. H. J., and Prins, R., *Catal. Lett.* **1**, 55 (1988).
37. Clausen, B. S., and Topsoe, H., *Hyper. Interact.* **47**, 203 (1989).
38. da Silva, P., IFP Thesis, 1998.
39. Wambecke, A., Toulhoat, H., Boutrois, J. P., Grimblot, J., and Bonnelle, J. P., *in* "Proceedings of the IVth International Symposium on the Scientific Bases for the Preparation of Heterogeneous Catalysts" (B. Delmon, *et al.*, Eds.), Studies in Surface Science and Catalysis Vol. 31, p. 581. 1987.
40. Raybaud, P., Hafner, J., Kresse, G., Kasztelan, S., and Toulhoat, H., "Proceedings of Hydrotreatment and Hydrocracking of Oil Fractions, Antwerpen" (B. Delmon *et al.*, Eds.), Studies in Surface Science and Catalysis Vol. 127, p. 309. 1999.